Activity and stability of the catalytic hydrogel membrane reactor for treating oxidized contaminants

Randal Marks [a], Joseph Seaman [b], Junyeol Kim [a], Kyle Doudrick [a, *]

[a] University of Notre Dame, Department of Civil and Environmental Engineering and Earth Sciences, USA
[b] University of Notre Dame, Department of Chemical and Biomolecular Engineering, USA

ARTICLE INFO

ABSTRACT

The catalytic hydrogel membrane reactor (CHMR) is an interfacial membrane process that uses nano-sized catalysts for the hydrogenation of oxidized contaminants in drinking water. In this study, the CHMR was operated as a continuous-flow reactor using nitrite (NO_2^-) as a model contaminant and palladium (Pd) as a model catalyst. Using the overall bulk reaction rate for NO_2^- reduction as a metric for catalytic activity, we evaluated the effect of the hydrogen gas (H_2) delivery method to the CHMR, the initial H_2 and NO_2^- concentrations, Pd density in the hydrogel, and the presence of Pd-deactivating species. The chemical stability of the catalytic hydrogel was evaluated in the presence of aqueous cations (H^+, Na^+, Ca^{2+}) and a mixture of ions in a hard groundwater. Delivering H_2 to the CHMR lumens using a vented operation mode, where the reactor is sealed and the lumens are periodically flushed to the atmosphere, allowed for a combination of a high H_2 consumption efficiency and catalytic activity. The overall reaction rate of NO_2^- was dependent on relative concentrations of H_2 and NO_2^- at catalytic sites, which was governed by both the chemical reaction and mass transport rates. The intrinsic catalytic reaction rate was combined with a counter-diffusional mass transport component in a 1-D computational model to describe the CHMR. Common Pd-deactivating species [sulfite, bisulfide, natural organic matter] hindered the reaction rate, but the hydrogel afforded some protection from deactivation compared to a batch suspension. No chemical degradation of the hydrogel structure was observed for a model water (pH > 4, Na^+, Ca^{2+}) and a hard groundwater after 21 days of exposure, attesting to its stability under natural water conditions.

© 2020 Elsevier Ltd. All rights reserved.

1. Introduction

Catalytic hydrogenation is an advanced reduction process used to treat oxidized contaminants in drinking water, including oxoanions (e.g., nitrate, nitrite, bromate, chlorate, perchlorate) (Guo et al., 2018; Heck et al., 2019; Li et al., 2019; Mahmudov et al., 2008; Pintar et al., 1996; Prusse and Vorlop, 2001; Qian et al., 2014; Shuai et al., 2013; Soares et al., 2008; Wong et al., 2009; Yoshinaga et al., 2002) and halogenated organics (e.g., trichloroethylene, dichloro-ethylene) (Chaplin et al., 2012; Davie et al., 2008; Fang et al., 2011; Heck et al., 2009; Hu et al., 2018; Li et al., 2012; Nutt et al., 2005; Zhao et al., 2013). Development of active and selective continuous

reactors is a critical need for implementation of catalytic hydro-genation as a treatment technique (Hu et al., 2018; Martinez et al., 2017). Traditional fixed-bed reactors (Bergquist et al., 2016; Bertoch et al., 2017; Choe et al., 2015; Pintar and Batista, 2007) and struc-tured catalyst support reactors [e.g., monoliths (Horold et al., 1993a, 1993b; Vorlop and Tacke, 1989), cloths (Matatov-Meytal and Sheintuch, 2005, 2009; Matatov-Meytal et al., 2000, 2001, 2003), and foams (Chinthaginjala et al., 2010; Espinosa and Lefferts, 2016)] immobilize the catalysts for continuous-flow operation, but they suffer from H_2 mass transfer limitations, effectively reducing the activity. Thus, there is a need for the development of alternative reactors.

Interfacial catalytic membrane reactors are a practical solution to address catalyst immobilization and mass transfer limitations (Centi et al., 2003; Daub et al., 1999; Dittmeyer et al., 2001, 2004; Espinosa et al., 2016, 2018; Holler et al., 2001; Strukul et al., 2000). They are composed of a membrane containing solid-phase catalyst particles that are in simultaneous contact with the gas and liquid

phases (i.e., triple-phase contact). The operational conditions of the gas (e.g., H_2) and aqueous phases can be independently controlled to meet reaction needs. In our previous study, we reported on the development of a new interfacial membrane reactor, the catalytic hydrogel membrane reactor (CHMR) (Marks et al., 2019). The CHMR consists of a central gas-permeable tubular hollow fiber membrane (HFM) that is coated with a hydrogel that immobilizes catalyst nanoparticles. The hydrogel matrix offers excellent diffusivity of aqueous species to minimize diffusive transport limitations (Puguan et al., 2015). The reductant H_2 is supplied through the HFM interior (i.e., the lumen) and diffuses through the HFM wall into the hydrogel, while the aqueous contaminants transport diffuse from the bulk solution through the exterior of the hydrogel. The overall reaction rate of the reactive species is governed by the inherent catalytic reaction rates and reactant diffusion rates through stagnant zones, including the HFM wall, the external liquid diffusion layer (LDL), and hydrogel (Dittmeyer et al., 2001; Marks et al., 2019; Nerenberg, 2016; Postma et al., 2018; Strukul et al., 2000). The Pd-loading density in the hydrogel has been shown to influence reaction rates and catalytic activity (Marks et al., 2019), but further investigation of reaction parameters is necessary to enable adoption of this technology, including techniques for H_2 delivery to the lumen, characterization of the effect of reactive species concentrations (e.g., NO_2^-, H_2) and catalyst inhibiting species on the catalytic activity, and the effect of water conditions on the structural stability of the hydrogel.

In systems that rely on bubbling H_2 into the aqueous phase (e.g., packed bed reactors), once saturation is reached increasing the flow rate will not affect the reaction rate. In contrast, for the CHMR, the reaction rate is controlled by the H_2 pressure in the lumen because this pressure controls the amount of available H_2 at catalytic sites (Dittmeyer et al., 2001; Espinosa et al., 2016, 2018). The molar ratio of H to aqueous contaminants at active sites controls catalytic activity and selectivity in hydrogenation reactions (Huai et al., 2015; Nakayama and Takahashi, 2015), and this ratio is greatly influenced by whether the H_2 is delivered co- or counter-diffusionally with respect to the contaminant(s) (Marks et al., 2019). The effect of H_2 lumen pressure on the kinetics of hydrogenation using a CHMR has yet to be evaluated.

Understanding how various aqueous species affect the activity of the catalyst is necessary to determine the range of water that can be treated using the CHMR. Catalysts immobilized in alginate have shown good stability in a range of aqueous conditions (Huang et al., 2016; Qiao et al., 2017; Xuan et al., 2017), and a CHMR containing Pd maintained its catalytic activity over an intermediate operation time in groundwater (i.e., 6 h) (Marks et al., 2019). But, the effect of known species that deactivate Pd [e.g., sulfite (SO_3^{2-}), bisulfide (HS^-), and natural organic matter (NOM) (Chaplin et al., 2006, 2012; Chen et al., 2013)] have not been explored for Pd nanoparticles that are embedded in a Ca-alginate matrix such as the CHMR.

The hydrogel coating used for catalyst immobilization provides key advantages over other structures, including its low cost, simple synthesis, and ability to vary the catalyst loading (Ai and Jiang, 2013; Ai et al., 2012; Chen et al., 2009; Chtchigrovsky et al., 2012; Li et al., 2015; Saha et al., 2010; Thangaraj et al., 2018). Furthermore, small aqueous molecules have a higher diffusivity through the hydrogel compared to traditional support structures (e.g., alumina) (Garbayo et al., 2002). For the CHMR to be considered for realistic use, the stability of the Ca-alginate hydrogel must be addressed. Ca-alginate is formed by ionically cross-linking Ca^{2+} with two guluronate residues to form a stable three-dimensional structure (Lee and Mooney, 2012). Ca-alginate is susceptible to chemical degradation through an ionic exchange reaction between monovalent cations (e.g., Na^+, H^+) and Ca^{2+} in cross-linked sites (Bajpai and

Sharma, 2004; Francis et al., 2013). At acidic pH, H^+ ions displace Ca^{2+} and hydrogel structural integrity decreases (Chuang et al., 2017). Yet to be determined is how the Ca-alginate hydrogel used for the CHMR responds to typical ranges of aqueous conditions in terms of structural stability and Pd leaching.

In this study, we describe the performance of the CHMR under continuous flow operation for hydrogenation of a model contaminant (NO_2^-) using a model catalyst (Pd), which is important for evaluation of the challenges relating to implementation of the CHMR for treatment of groundwater. Specifically, this study evaluated the effect of (i) the H_2 delivery mode to the CHMR on the catalytic activity and H_2 consumption efficiency, (ii) the initial reactant species concentrations (NO_2^-, H_2) on the catalytic activity, (iii) the presence of ions on the hydrogel stability, and (iv) deactivating species (SO_3^{2-}, HS^-, and NOM) on the long-term activity of Pd. Finally, a 1-D model was developed that can be used to relate observed reaction kinetics to concentration profiles that develop within the catalytic hydrogel during reaction.

2. Materials and methods

2.1. Assembly of the CHMR

The catalytic hydrogels were synthesized using a previously reported method (Marks et al., 2019), and detailed descriptions of the synthesis procedure can be found in the Supporting Information (S). Briefly, 2% (w/w) alginic acid, sodium salt (low viscosity, #01469, Chem-Implex Inc.) was dissolved in ultrapure water (18.2 MΩ-cm). A 25-cm length of the silicone HFM (0.037″ OD x 0.025″ ID, #025BRA002, Braintree Scientific, Saint Gobain) was completely submerged in the alginate solution in a custom-built half-tube reactor. A 20-mL cross-linking solution (100 mM total concentration) was prepared by dissolving calcium chloride ($CaCl_2$, anhydrous, #C77, Fisher Scientific) and palladium nitrate dihydrate ($Pd(NO_3)_2 \cdot 2H_2O$, #76070, Sigma Aldrich) in aqueous solution, which was then poured into a separate half-tube reactor. The alginate-coated membrane was removed from the alginate solution and rapidly transferred to the Ca^{2+}/Pd^{2+} cross-linking solution for 30 min. This procedure was repeated once to increase the hydrogel thickness and stability. The embedded Pd^{2+} was reduced to Pd nanoparticles by then submerging the coated HFMs in 2.5 mM sodium borohydride ($NaBH_4$, 98%, #13432, Alfa-Aesar).

To construct a multifiber CHMR, eight catalytic hydrogel membrane (CHM) strands were inserted in a 25-cm long plastic tube with an inner diameter of 1.27 cm (Fig. S1). Plastic T-connectors were installed on both ends of the tubing and the uncoated HFM ends of the CHMs were fixed in place with adhesive (urethane, #2RUD4, Grainger) to create a water-tight seal. Special care was taken to ensure the HFM openings were not crimped or sealed. The Pd mass in the CHMs and aqueous solution was quantified using acid microwave digestion and inductively coupled plasma-optical emission spectroscopy (see SI for further details) (Marks et al., 2019).

2.2. Continuous-flow reactor configuration

To conduct NO_2^- hydrogenation experiments, the CHMR was configured as a continuous-flow reactor with recycle (Fig. 1). NO_2^- was added to the influent reservoir (1000 mL) at varying concentrations. The reactor pH was buffered (5.8−6.3) by bubbling carbon dioxide (CO_2, #CD75, American Gas and Welding) at 100 mL/min and by addition of 10 mM sodium bicarbonate ($NaHCO_3$, ACS grade, #41900068-1, bio-world) into the influent reservoir. To counteract the possibility of the Na^+ ions de-linking the Ca-alginate hydrogel, 1.4 mM calcium chloride ($CaCl_2$, anhydrous, C77-500, Fisher
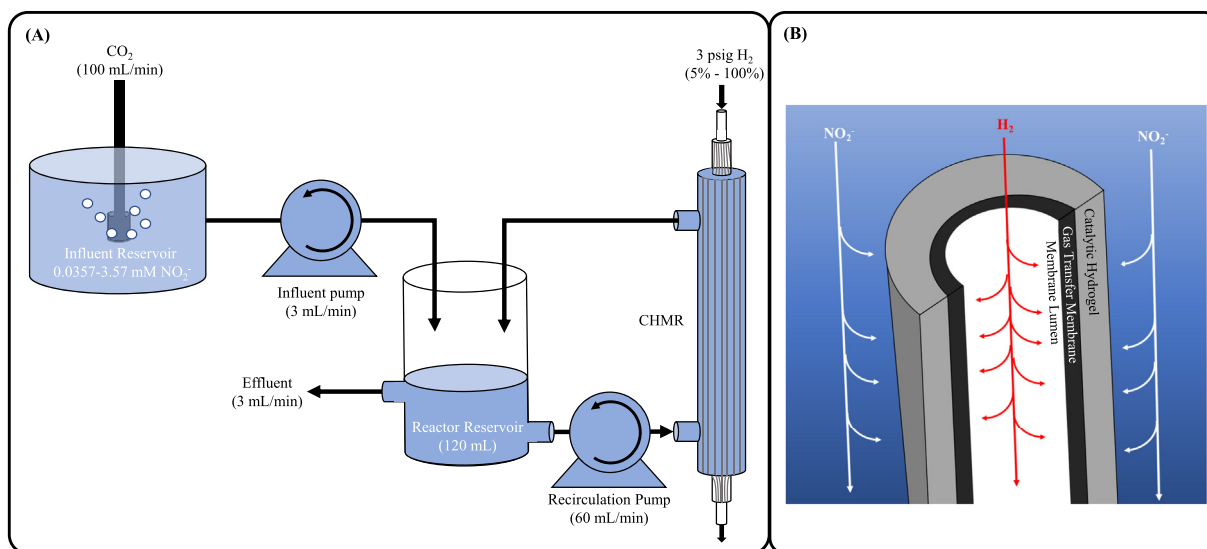
Fig. 1. (A) Schematic of reactor configuration including selected reactor parameters. (B) Magnified schematic of a single CHM within the reactor showing the counter-diffusional delivery of NO_2^- and H_2 to the catalytic hydrogel.

Scientific) was also added. The influent reservoir was fed to a reactor reservoir (120 mL) by a peristaltic pump (3 mL/min). The reactor reservoir had two outlets. The first outlet led to the CHMR and this was recycled through the CHMR and back into the reactor reservoir using a peristaltic pump (60 mL/min, liquid velocity 2.4 cm s^{-1}). The flowrate was chosen to establish a recycle ratio of 20 so the overall behavior of the system was comparable to a completely stirred reactor. The second outlet was the system effluent (at water level) and the flowrate matched the influent flowrate (3 mL/min), creating a hydraulic retention time in the combined CHMR and reactor reservoir of 40 min. Unless otherwise noted, all experiments were conducted in this reactor configuration.

Reaction conditions for a typical experiment are listed in Table S1. In all experiments, the pumps were first turned on until the CHMR volume was full and liquid was detected in the effluent. Then, at t = 0, hydrogenation (the reaction) was initiated by supplying H_2 at 3 psig (1.22 bar) to the CHMR through the HFM lumen. NO_2^- and NH_4^+ concentrations were measured in the effluent at regular intervals using ion chromatography (IC; Dionex ICS 5000+, AS-23 column, CS-12A column).

2.3. Effect of the H_2 delivery mode

The effect of the H_2 delivery mode on the NO_2^- reduction activity and the H_2 consumption efficiency was evaluated by running the CHMR in closed, open, and vented modes. A valve was installed at the end of the HFM to control the release of H_2 to the atmosphere. For all experiments, 1.78 mM NO_2^- (NaNO$_2$, reagent grade, #0535, VWR) was provided in the aqueous influent and 3 psig (1.22 bar) of 100% H_2 (ultra-high purity, #HY-UHPT, American Gas and Welding) was supplied to the HFM lumen. For open mode operation, experiments were conducted with the valve open, which allowed all H_2 not diffusing through the HFM wall to exit to the atmosphere. Using a flow meter, the H_2 flowrate in open mode was measured to be approximately 4 L min^{-1} at 3 psig. For closed mode operation, the valve was closed to prevent the escape of H_2 from the lumen end, so H_2 could only leave by diffusing through the HFM wall. For the vented mode experiment, the valve was opened every 15 min for 5 s.

2.4. Effect of reactant species concentrations

The effect of NO_2^- and H_2 concentrations on the catalytic activity was investigated by varying the influent NO_2^- concentrations (0.357−3.57 mM) and the percent H_2 (5−100%, pre-mixed with N_2, ultrahigh purity, American Gas and Welding) provided to the lumen during catalytic hydrogenation in open mode using the reactor configuration described previously. All experiments were operated until steady-state was achieved, as confirmed by periodic measurement of NO_2^- concentrations in the reactor effluent. All equations used to calculate the NO_2^- conversion and rate constants are provided in the SI.

2.5. Effect of catalyst deactivating species

SO_3^{2-}, HS^-, and NOM were used to evaluate their effect on the NO_2^- reduction activity caused by catalyst deactivation. In each experiment, the influent reservoir contained 1.78 mM NaNO$_2$, 10 mM NaHCO$_3$, and 1.4 mM CaCl$_2$. The CHMR was operated until steady-state conditions were reached with respect to NO_2^- reduction. Then, the influent reservoir was spiked with one of the species causing deactivation: 5 mg-S/L sodium sulfite nonahydrate (Na$_2$SO$_3$, anhydrous, AA65122-14, Alfa Aesar) or 1 mg-S/L sodium sulfide (Na$_2$S· 9H$_2$O, 98%, #BJ208043, Fluka), or 5 mg/L Suwanee River NOM (2R101N, International Humic Substances Society). The effect of the deactivating species was evaluated for up to 15 h by periodic sampling of NO_2^- for subsequent IC analysis. For the SO_3^{2-} and NOM experiments, CO_2 was bubbled in the influent reservoir to buffer the pH to ~5.8. For HS^-, no CO_2 was used and the pH was kept at ~8.2 to avoid formation of H_2S (pK$_a$ = 7.02).

2.6. Batch suspension reactions using recovered Pd nanoparticles

Pd nanoparticles were first isolated from the hydrogels by dissolving the Ca-alginate in a solution of ethylenediaminetetraacetic acid (EDTA, 0.1 M) and sodium citrate (0.2 M). The particles were recovered by centrifugation with intermittent washing with ultrapure water (n = 3). For the batch experiments, Pd nanoparticles (1.13 and 4.87 mg) were suspended in a 60-mL solution containing NaNO$_2$ (1.78 mM), NaHCO$_3$ (10 mM), and CaCl$_2$ (1.4 mM). CO_2 (100 mL/min) and H_2 (150 mL/min) were bubbled continuously into

the reactor. Pd masses similar to those used in the CHMR experiments (low and high loadings) were used. Periodic aqueous samples were taken, filtered, and then the NO_2^- and NH_4^+ concentrations were analyzed using IC. All batch experiments were repeated using 1.13 mg Pd in the presence of the deactivating species (i.e., Section 2.5, same concentrations).

2.7. Effect of co-ions on the stability of the hydrogel

The stability of the Ca-alginate hydrogel in the presence of de-linking ions (H^+, Na^+) was investigated by exposing Ca-alginate hydrogels to various aqueous conditions. Ca-alginate hydrogels were grown on HFMs as described previously and then submerged in vessels containing an aqueous solution of desired composition for 7 d. No mixing was used so that only chemical stability changes were observed. The changes in the concentrations of Ca^{2+} and Pd in aqueous solution and the CHM mass were used as metrics for evaluating the stability. The change in the CHM mass is reported as a mass ratio, equal to the CHM wet mass in ultrapure water (at equilibrium) divided by the CHM wet mass after being exposed to selected aqueous conditions for 7 d. The mass ratio indicates shrinking or swelling of the hydrogel structure due to changes in the total number of crosslinked sites. The conditions evaluated in the 7 d experiments were: 0.5, 5, and 50 mM total concentration of either NaCl, $CaCl_2$, or NaCl + $CaCl_2$ (10:1.4 M ratio). Additional hydrogel stability experiments were conducted by exposing the CHM to a hard groundwater for 21 d and comparing the results to ultrapure water. The groundwater characterization and full experimental details are given in the SI.

3. Results & discussion

3.1. Effects of the hydrogen delivery mode on catalytic activity

Independent control of the H_2 delivery into the lumen is a critical aspect of the CHMR due to the influence of the H_2 concentration on the catalytic activity and byproduct selectivity. H_2 delivery can be achieved through different modes that will influence the H_2 concentration in the catalytic hydrogel and H_2 consumption efficiency. In "closed mode," the HFM is sealed at the end and all H_2 that enters can only leave by diffusion through the HFM wall. H_2 consumption efficiencies in this mode approach 100% since all H_2 must pass into the catalytic hydrogel where reaction occurs (Ahmed et al., 2004; Martin and Nerenberg, 2012; Pankhania et al., 1994; Perez-Calleja et al., 2017). The drawback to closed mode is back-diffusion of non-reactive gases (i.e., CO_2, N_2) from the aqueous phase into the sealed membrane. Back-diffusion results in an H_2 gradient along the lumen length (i.e., lower H_2 at one end), and therefore in the hydrogel, which lowers the catalytic activity of the CHMR. In "open mode," the HFM is open at the end, and all the H_2 that does not diffuse through the HFM wall exits the HFM into the atmosphere. This mode is used to prevent formation of the unwanted H_2 gradients, and it improves catalytic activity, but causes a low H_2 consumption efficiency. The final option is a mixture of closed and open modes, called "vented mode," which is a strategy initially developed for membrane biofilm reactors (Perez-Calleja et al., 2017). For vented mode, the HFM is set up similar to closed mode, but a valve is placed at the end of the HFM to allow it to be opened at regular intervals to flush out the inert gases. This mode maintains a consistent H_2 partial pressure throughout the HFM while ensuring good H_2 consumption efficiency. In this study, a conservative vent cycle of 15 min closed followed by 5 s open was selected to maximize activity, limit H_2 gradient formation in the lumen, and allow pseudo-steady state conditions to develop in the CHMR.

The results of the NO_2^- hydrogenation experiments operated in open, closed, and vented modes in shown in Fig. 2. At the beginning of hydrogenation, the effluent NO_2^- concentration is equal to the influent concentration, and the effluent concentration continuously decreases until steady state is achieved. Steady-state conditions were reached within 2.5 h for all operation modes. The average NO_2^- conversion at steady-state for open, closed, and vented modes was 64.5 ± 0.6%, 4.0 ± 0.4%, and 56.8 ± 1.1%, respectively. In closed mode, the NO_2^- conversion was greatest at the first time point as the H_2/inert gas gradient had not yet fully developed. As the reaction proceeded, the conversion decreased as the gradient in the lumen fully developed, stabilizing within 2 h. Conversions were comparable between open and vented modes, suggesting their H_2 concentrations were similar in the catalytic hydrogel. The standard deviation of the average conversion was higher in vented mode compared to open and closed modes due to the repeated development of transient H_2 gradients during the 15-min periods between venting, which prevented a true steady-state from occurring.

The H_2 consumption efficiency can be determined by evaluating the ratio of H_2 consumed by reaction with NO_2^- to the total volume released from the supplying tank during the reaction period (calculations in SI). During a 1-hr steady-state period, approximately 0.039, 0.62, and 0.54 mmol of H_2 were consumed by the reaction in closed, open, and vented modes, respectively. In closed mode, the H_2 consumption efficiency approached 100% because all H_2 was assumed to leave the lumen only by diffusion. In open mode, most of the H_2 was released to the atmosphere (~9809 mmol/h), so a low consumption efficiency of 0.0064% was observed. In vented mode, 54.4 mmol of H_2 exited the lumen during the four open venting cycles per hour, resulting in an H_2 consumption efficiency of approximately 1.0%. While this efficiency is still low compared to closed mode, the NO_2^- removal was much higher, providing an excellent compromise between catalytic performance and H_2 consumption efficiency. Operation of the CHMR in vented mode can be improved with an optimized venting scheme (i.e., reduce vent time) that minimizes H_2 gradient formation and loss of H_2 through the lumen end as well as improving the H_2 consumption efficiency. All further experiments in this study were conducted in open mode to simplify reactor conditions and remove extraneous processes (e.g., formation of H_2 gradients).

3.2. Effects of the reactive species concentration on NO_2^- hydrogenation

Evaluating the effect of the influent concentration of the reactive species (i.e. H_2, NO_2^-) on the reaction rate is critical for
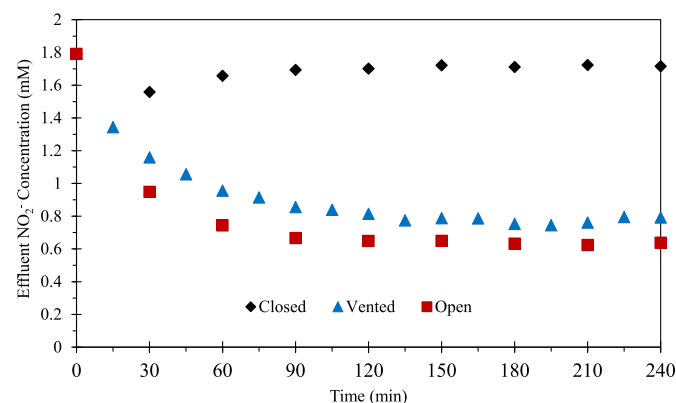

Fig. 2. Continuous-flow operation of a CHMR under open, closed, and vented operation modes for H_2 supply. The hydraulic retention time was 40 min.

understanding the limiting reactions of the CHMR. A batch experiment using suspended catalysts was first run to determine the reaction rate on the catalyst without interference from mass transport limitations. These kinetic results confirmed that NO_2^- reduction followed pseudo first-order behavior on Pd (Fig. S2). Continuous-flow CHMR experiments were then conducted in open mode using a range of influent NO_2^- (0.357−3.57 mM) and H_2 concentrations (5−100% in N_2). Two Pd-loadings (low: 2.26 mg; high: 9.70 mg) were selected to evaluate the effect of the number of active sites on the reaction rate.

Fig. 3A and B present the reaction rate, r', for a range of H_2 concentrations as a function of effluent NO_2^- concentrations (i.e., steady-state) for the high and low Pd-loadings, respectively. r' is the reaction rate normalized to Pd molarity (i.e., mol-N mol-Pd^{-1} s^{-1}) and is obtained from the from the steady-state continuous-flow experiments (Table S2). For all conditions, r' increased with increasing H_2 and NO_2^- concentrations, and r' for the low Pd-loading was higher at all conditions compared to the high Pd-loading. Because the curve slopes were not linear and different rates were observed for the H_2 variations under otherwise similar conditions, the overall reaction rate was not strictly first-order and the rate was be dependent on the number of active Pd sites, the concentration of H_2, and the NO_2^- concentration.

Fig. 3C and D present Pd normalized NO_2^- conversion for a range of H_2 concentrations as a function of effluent NO_2^- concentrations for the high and low loadings, respectively. Similar to trends observed for r' (i.e., Fig. 3A and B), a higher influent H_2 concentration and a lower Pd-loading achieved the greatest the Pd

normalized NO_2^- conversion, but an opposite trend was observed for the steady-state NO_2^- concentration. Increasing the influent NO_2^- concentration generally decreased the NO_2^- conversion, except for the 25, 50, and 100% H_2 conditions of the low loading, where the conversion initially increased and then decreased with increasing NO_2^- concentration. This observation in conjunction with the slope of the reaction rate curves indicates that the reaction order shifts between zero and first order.

Heterogeneous catalysis reactions are typically described by Langmuir-Hinshelwood kinetics (Chaplin et al., 2006; Jani et al., 2012; Pintar et al., 1996, 1998); however, due to the mass transfer effect imparted by the hydrogel, this model does not appropriately describe the observed reaction rate of the CHMR. This was evident when comparing the observed reaction rate, r (i.e., without Pd normalization; Table S2) to the r' values of the high (Fig. 3A) and low Pd (Fig. 3B) loading results. The observed reaction rate was greater for the high Pd-loading compared to the low loading, but because the low loading had a higher r', this indicates that it had a wider reactive zone that used a larger percent of the Pd, as discussed previously (Marks et al., 2019).

To evaluate the effect of diffusion limitations within the CHMR, the Pd-normalized first-order rate constant, k_1', of the batch (Fig. S2) and CHMR experiments were used to calculate the activity ratio. The activity ratio is a measure activity loss in the CHMR due to mass transfer limitations, calculated by dividing k'_{CHMR} by k'_{batch}. The k_1' for the low and high Pd-loadings of the CHMR were 1.32 and 0.667 L mol-Pd^{-1} s^{-1}, respectively. In the batch system, the k_1' for equivalent low and high loadings were 1.40 and 1.08 mol-Pd^{-1} s^{-1},
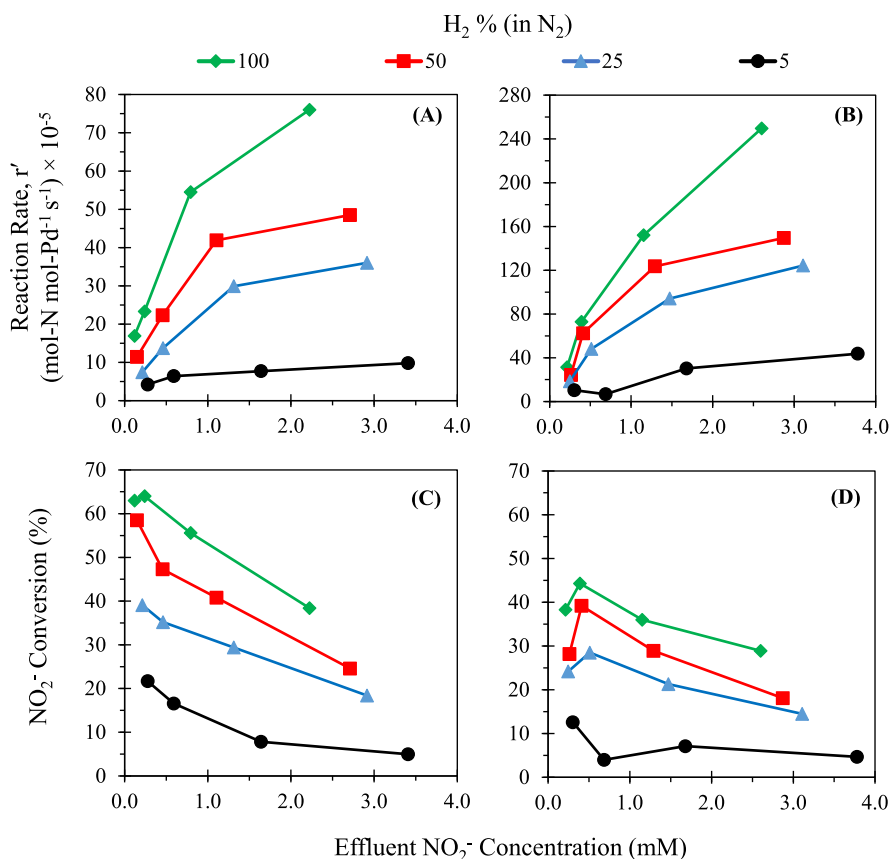

Fig. 3. Results of NO_2^- hydrogenation kinetic experiments. The Pd-molarity normalized reaction rate (r') over a range of influent H_2 percentages (in N_2) as a function of effluent NO_2^- (i.e., steady-state) concentrations are presented for (A) a 9.70 mg Pd-loaded CHMR (high loading) and (B) a 2.26 mg Pd-loaded CHMR (low loading). The NO_2^- conversion for a range of influent H_2 percentages (in N_2) as a function of effluent NO_2^- concentrations are presented for (C) a 9.70 mg Pd-loaded CHMR and (D) a 2.26 mg Pd-loaded CHMR. All plots are a function of effluent NO_2^- concentration because this is the approximate concentration in the well-mixed reactor at steady-state. The legend at the top indicates the H_2 percentage.

respectively. The corresponding activity ratios for the low and high Pd-loadings were 0.94 and 0.62, respectively. This correlation confirms the role of mass transport in limiting the reaction rates, especially in the case of the high loading, where the reactive zone was small and confined near the bulk solution. This finding was consistent with observations in our previous study (Marks et al., 2019), where more densely loaded CHMs had a lower activity ratio due to slow diffusive transport of NO_2^- to active Pd sites deep within the hydrogel.

While a first-order rate constant does not accurately reflect the overall reaction rate behavior for the range of conditions tested in this study, a maximum k_1' was calculated to allow for general comparisons across other studies that report k_1' [i.e., Tables S2 and S3 (Bertoch et al., 2017; Espinosa et al., 2018; Holler et al., 2001; Jarrah, 2018)]. A k' of 1.87 L mol-Pd^{-1} s^{-1} was calculated for the low Pd-loading at an H_2 partial pressure of 1.22 bar (i.e., 100%) and an influent NO_2^- concentration of 0.71 mM, which is approximately two orders of magnitude greater than the rate constants reported in our previous study on the CHMR that used closed mode and no CO_2 buffer, attesting to their operational importance (Marks et al., 2019). Though the byproduct selectivity was not a focus of this study, NH_4^+ concentrations were measured to provide insight into the effect of initial H_2 and NO_2^- concentrations. Generally, the NH_4^+ selectivity (Table S2, Fig. 4) decreased as the H/N ratio decreased and remained below 5% under high influent NO_2^- concentrations, consistent with previous results (Marks et al., 2019; Postma et al., 2018; Zhao et al., 2016). This result attests to the ability of the CHMR to easily alter the byproduct selectivity by adjusting the H_2 partial pressure.

3.3. Evaluating effects of diffusion limitations using a 1-D computational model

NO_2^- hydrogenation at Pd sites has been shown to best fit the Hinshelwood steady-state adsorption (SSA) kinetic model proposed (Hinshelwood, 1940; Pintar et al., 1998; Shelstad et al., 1960), wherein H_2 adsorbs and dissociates on the Pd surface before reacting with aqueous NO_2^- in the outer Helmholtz plane to form either NH_4^+ or N_2. In this study, the proposed causative factor for activity loss with increasing NO_2^- concentrations is from transport limitations of NO_2^- within the catalytic hydrogel. To account for the

mass transport limitations in the overall reaction rate, a 1-D model was created using the AQUASIM simulation program based on membrane biofilm reactors (Martin et al., 2013) and incorporating the Hinshelwood SSA kinetic model for the intrinsic NO_2^- reaction rate. The model was used to conceptualize the concentration profiles of NO_2^- and H_2 within the hydrogel.

When supplied with influent NO_2^- concentrations and H_2 partial pressure in the lumen, the model predicts NO_2^- removal at steady-state and the concentration profiles of reactive species within the hydrogel. The location and thickness of the reactive zone (RZ; region of the catalytic hydrogel where H_2 and NO_2^- interact at active catalyst active sites) can be estimated using the model and related to observed reaction kinetics. The model considers diffusion of H_2 from the lumen through the HFM wall and into the hydrogel, diffusion of NO_2^- from the bulk aqueous zone through the stagnant LDL and into the hydrogel, and the catalytic reaction of NO_2^- and H_2 in the RZ. The modeled reactor configuration (hydraulic retention time, reactor volume, hydrogel properties, etc.; Table S1) was taken from this study, and the chemical and physical parameters (reaction kinetic model and diffusion coefficients) were taken from previous studies (Martin et al., 2015; Pintar et al., 1998). This simplified model describes the effect of only H_2 and NO_2^- concentrations and is used herein only as a conceptual tool to elucidate the observed experimental results. Details on the model configuration and descriptive equations can be found in the SI.

Fig. 5 shows the model output of the concentration profiles of NO_2^- and H_2 at steady-state conditions. H_2 diffuses from the HFM wall into the hydrogel, where a concentration profile develops that is dependent on both diffusive transport and catalytic reaction. A similar, but counter-diffusional, profile develops for NO_2^-, as it diffuses from the bulk through the LDL and into the hydrogel, where it is also subject to both reaction and diffusion processes. As the H_2 partial pressure in the lumen increases with a constant influent NO_2^- concentration, the concentration profile shape of both NO_2^- and H_2 within the hydrogel change (Fig. 5A). At the lowest H_2 partial pressures, H_2 is rapidly consumed by reaction as it leaves the HFM wall and travels into the hydrogel. The RZ (gray region) is made up of only a small fraction of the portion of the hydrogel nearest the HFM wall. NO_2^- fully penetrates the hydrogel and the NO_2^- concentration within the hydrogel is relatively constant, suggesting low catalytic reaction rates and confirms the low NO_2^-
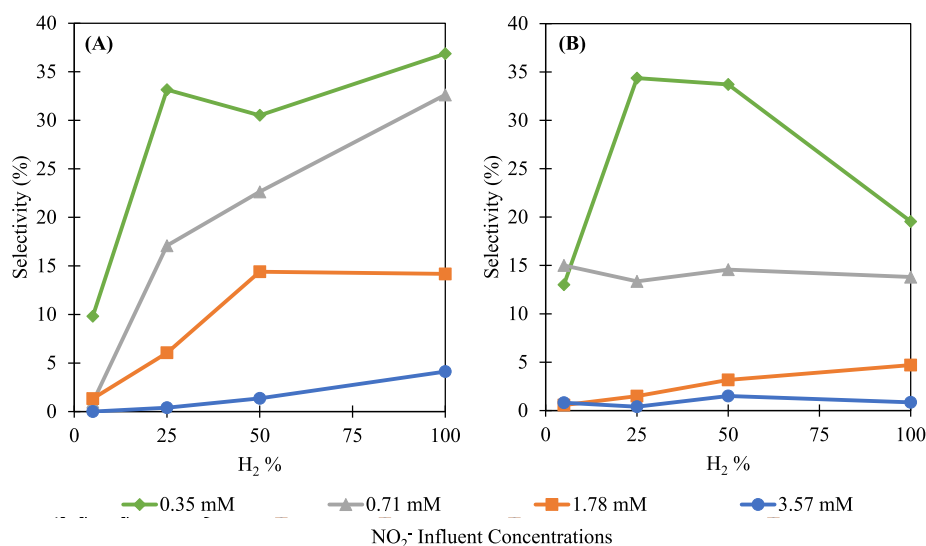

Fig. 4. Steady-state NH_4^+ selectivity for NO_2^- hydrogenation over a range of influent NO_2^- concentrations and H_2 percent mixtures for (A) 9.7 mg Pd-loaded membrane and (B) 2.26 mg Pd-loaded membrane.
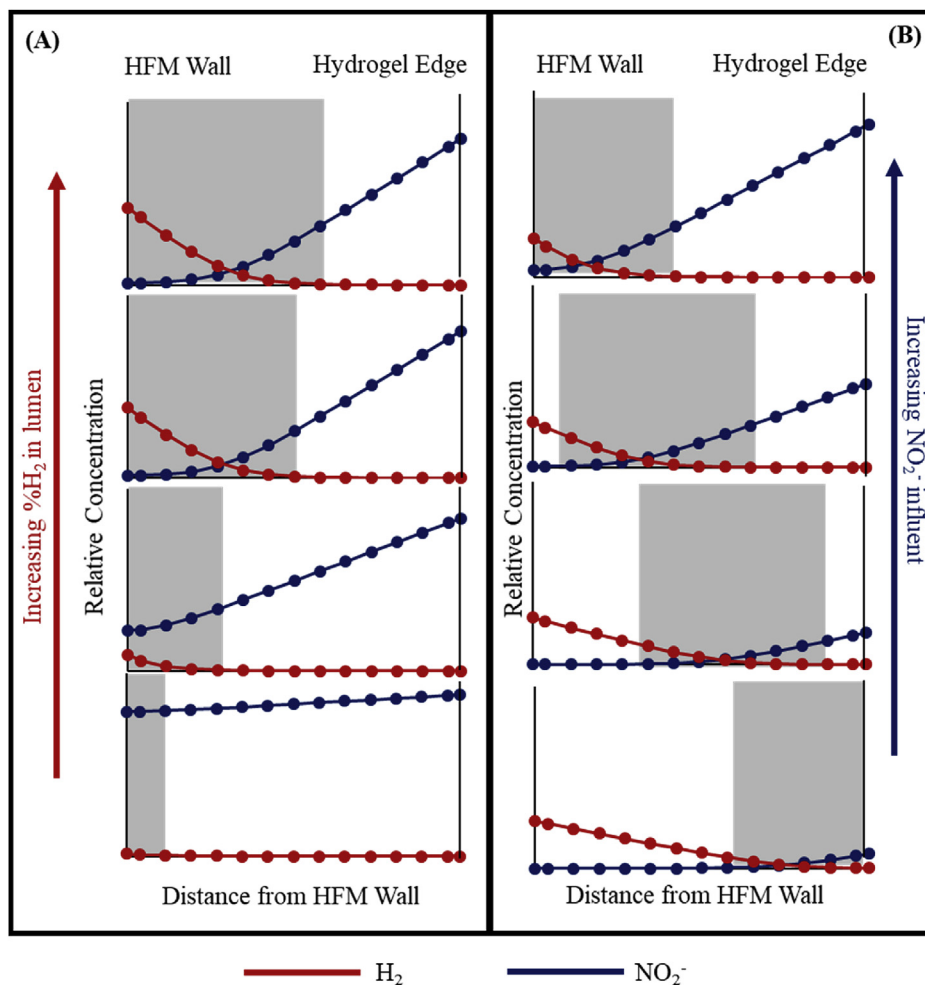
Fig. 5. Conceptual model of NO_2^- and H_2 concentration profiles within a CHM. Concentration of NO_2^- and H_2 as a function of position in the catalytic hydrogel is given over a range of conditions. Gray boxes indicate the position of the RZ within the hydrogel. Beyond the hydrogel edge is the LDL and bulk aqueous regions (not shown). (A) The effect of increased H_2% in the lumen while the influent NO_2^- concentration is held constant. (B) The effect of increased NO_2^- concentrations while H_2% in the lumen is held constant.

removal rates observed experimentally. As H_2 concentrations increase, H_2 penetrates deeper into the hydrogel towards the bulk before it is completely consumed by reaction with NO_2^-. The increased presence of H_2 throughout the membrane generates a quicker reaction rate, causing an increase in the NO_2^- concentration gradient as NO_2^- is more rapidly consumed. Further, the RZ expands and shifts towards the hydrogel exterior as the H_2 partial pressure increases, decreasing the average diffusive transport distance for NO_2^- before reaction. At the highest H_2 concentrations, the diffusive transport distance for NO_2^- to enter the RZ is minimized and NO_2^- reaction rates are maximized. The observed concentration profile changes with increasing reactive species concentrations correlate well with the shifts in experimentally measured r' with changes in reactive species concentration.

When NO_2^- influent concentrations are increased at constant H_2 pressure, concentration profiles shift in a corresponding manner (Fig. 5B). At the lowest NO_2^- concentration, all NO_2^- is consumed in a shallow RZ near the hydrogel edge, as H_2 diffuses across much of the hydrogel towards the bulk before reaching NO_2^- species. Increasing the NO_2^- concentration causes the RZ to move deeper into the hydrogel as NO_2^- diffuses further before being consumed by reaction. Finally, at the highest NO_2^- concentration, NO_2^- penetrates the entirety of the catalytic hydrogel without being fully consumed, while all H_2 is consumed rapidly near the HFM wall. As NO_2^- concentrations increase, the diffusive transport distance of NO_2^-

through the hydrogel to the RZ increases. Diffusive mass transport limitations become progressively more influential on overall kinetics as insufficient H_2 is delivered to the catalytic hydrogel through the lumen wall to fully reduce NO_2^- and removal rates no longer increase with increased NO_2^- concentrations. This trend corresponds well with the experimental results observed in Fig. 3, where increases in the NO_2^- influent concentration increases r' until a limit is reached that is dependent on the %H_2, confirming the role of diffusive transport on limiting the observed reaction rates.

The 1-D model is useful for describing the behavior of the CHMR. Continuing work should focus on calibrating the model with experimental data so that it can be used to identify key factors impacting the behavior of the CHMR (e.g., flux), including hydrogel catalyst density, H_2 supply pressure, influent and bulk NO_2^- concentrations, and hydrogel thickness.

3.4. Effects of select co-occurring species on the catalytic activity

One of the major challenges for catalytic hydrogenation is deactivation of the catalyst by other species in real waters. Our previous work showed that catalytic deactivation was minimal over a 3-day reaction period in a hard groundwater containing a relatively high SO_4^{2-} concentration, suggesting that the catalytic hydrogel may limit deactivation (Marks et al., 2019). To investigate the effects of known Pd deactivating species on the catalytic activity

of the CHMR, experiments were conducted in the presence of SO_3^{2-}, HS^-, and NOM for at least 12 h (Fig. 6). The addition of SO_3^{2-} (5 mg-S/L) resulted in a steady loss of conversion from 61.5% to 50.9%, indicating deactivation of the catalyst (Fig. 6A). A similar behavior was observed when HS^- (1 mg-S/L) was spiked into the reactor in a separate experiment (Fig. 6B). The initial steady-state conversion was lower than the other species because CO_2 was not used to prevent the formation of H_2S at acidic pH. Conversion in the absence of HS^- and CO_2 was 21.8%, and this steadily decreased to 2.5% after HS^- was spiked into the reactor (Fig. 6B), indicating deactivation had occurred. For NOM (5 mg/L), a different trend was observed compared to the other species. Initially after adding NOM, the conversion dropped from 60.3% to 46.8% after 2.5 h, but the conversion returned to 58.4% after an additional 12 h of exposure (Fig. 6C). This behavior suggests that the deactivating effects of NOM in the CHMR were temporary. The effect of these species on the catalytic activity of Pd is supported by previous results (Chaplin et al., 2006), but these results provide evidence that some protection from deactivation is provided by the hydrogel, especially in the case of NOM.

To determine the role of the hydrogel, the effect of these deactivating species on the intrinsic catalytic activity of the Pd nanoparticles in the absence of a hydrogel was evaluated using suspended batch reactor experiments (Fig. S3A). In the absence of deactivating species, the k' was L mol-Pd^{-1} s^{-1}, and this decreased to 0.648 and 0.299 L mol-Pd^{-1} s^{-1} in the presence of SO_3^{2-} and NOM, respectively. When HS^- was present, no NO_2^- removal was observed, suggesting that HS^- had severely deactivated the catalyst; however, poor removal was observed even when no HS^- was present (Fig. S3B) due to the high pH (pH$_{final}$ ≈ 9.5) when no CO_2

was used. These results are consistent with previous studies evaluating the effects of these deactivating species on Pd catalysts (Chaplin et al., 2006; Seraj et al., 2017; Xiao et al., 1992). Pd deactivation by sulfur compounds remains a challenge, but regeneration of the catalyst is a feasible approach (Chaplin et al., 2009). The cause of the reduced deactivation effect of NOM using the CHMR is less clear. Batch experiments with suspended particles showed that NOM deactivated Pd somewhat, but it was lower in the CHMR. This result suggests that the hydrogel prevented NOM-Pd interactions, which may be related to the poor transport of the NOM through the hydrogel.

3.5. Hydrogel stability as a function of aqueous conditions

The long-term stability of the Ca-alginate hydrogel is a critical challenge to implementation of CHMRs for treatment of drinking water. Fig. 7 shows the stability of hydrogels coated on HFMs or a range of aqueous conditions relevant to water treatment. The effect of pH on stability of Ca-alginate hydrogels (no Pd) was evaluated between neutral and acidic pH (Fig. 7A). Below pH 4, Ca^{2+} was released from the hydrogel, consistent with the protonation of guluronic (pK$_a$ = 3.65) and mannuronic (pK$_a$ = 3.38) acid moieties of alginate and the transition of the Ca-alginate to alginic acid (Chuang et al., 2017). The expulsion of Ca^{2+} from the hydrogel crosslink sites caused the gel to shift from transparent to opaque, as the chemical structure transitions from ionically bound Ca-alginate to alginic acid gel stabilized by hydrogen bonding (Draget et al., 2006). This transition hampered attempts to investigate catalytic function at acidic pH because the resulting alginic acid gel degraded rapidly due to mixing shear forces. Thus, limiting the aqueous pH above the pK$_a$ of alginic functional groups is critical to long-term stability and catalytic performance of Ca-alginate based CHMR. Operation at pH 5.8—6.3, as conducted in this study, provided an optimal catalytic activity while preventing instability of the Ca-alginate hydrogel.

Ionic exchange of monovalent cations (e.g., Na^+) with Ca^{2+} at crosslink sites can eliminate connections between polymer strands and break down the 3D structure of the hydrogel (Loureiro dos Santos, 2017). To investigate the effects of monovalent cations on the hydrogel stability and behavior, the mass ratio of CHMs was measured after exposure to solutions of increasing total concentrations of either Na^+ only, Ca^{2+} only, or a mixture of Na^+ and Ca^{2+} (Fig. 7B). When only Na^+ was present, the hydrogel swelled proportionally to the concentration of Na^+, indicating a loss of Ca-alginate crosslinked sites as Na^+ exchanged with Ca^{2+}. The addition of Ca^{2+} to the aqueous phase prevented swelling of the hydrogel, which was attributed to the affinity of alginate sites for the Ca^{2+} (Idota et al., 2016). When both Na^+ and Ca^{2+} were present at a total concentration of 50 mM (43.8 mM Na^+, 6.14 mM Ca^{2+}; 10:1.4 M ratio), the hydrogel shrank due to crosslinking of new sites from the additional Ca^{2+} (Matyash et al., 2014). These sites were likely initially filled by Pd^{2+} species prior to reduction to Pd^0, thus leaving them open. Indeed, when no Na^+ was present, hydrogel shrinking was observed even at low Ca^{2+} concentrations (e.g., <0.5 mM). Overall, the mass-ratio results showed that hydrogel swelling was dependent on the concentration and valence of cations in the aqueous phase. Shrinking and/or swelling of the hydrogel influences the overall catalytic performance of the CHMR. For example, shrinking results in an increased hydrogel density and a smaller pore network that will decrease the diffusivity of aqueous species (Favre et al., 2001; Pasut et al., 2008). This shrinkage could negatively influence the mass transport, and thus the overall reaction rate. Though, shrinking will also result in a decreased hydrogel thickness, which would improve the mass transport of the system (i.e., Fig. 5). The two phenomena work against each other,
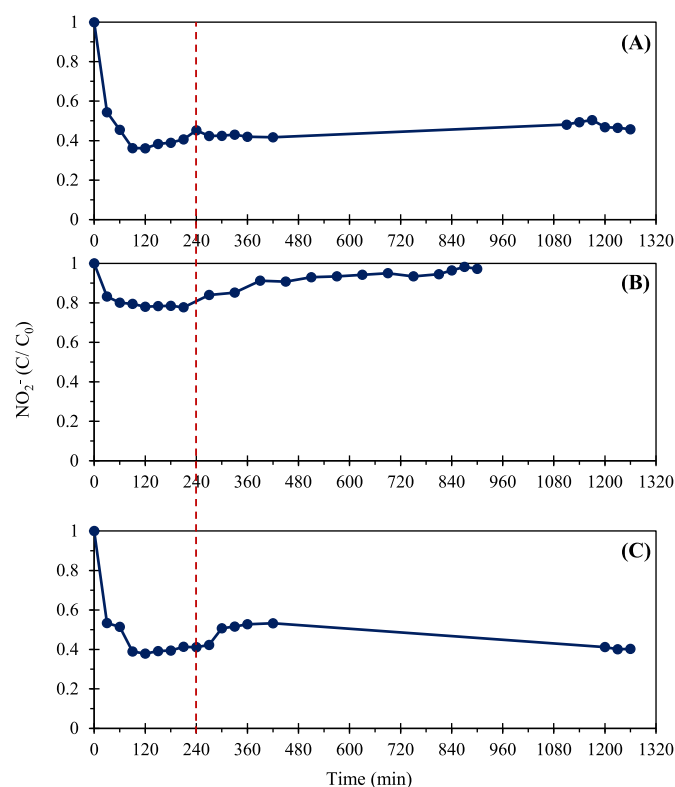

Fig. 6. Long-term continuous operation of a CHMR in the presence of known deactivation species (A) 5 mg-S/L SO_3^{2-}, (B) 1 mg-S/L HS^-, and (C) 5 mg/L NOM. The HS^- experiment was conducted in the absence CO_2 to avoid acidic pH and the formation of H_2S. The vertical red dashed line represents the timepoint when the species was spiked into the influent reservoir. (For interpretation of the references to colour in this figure legend, the reader is referred to the Web version of this article.)
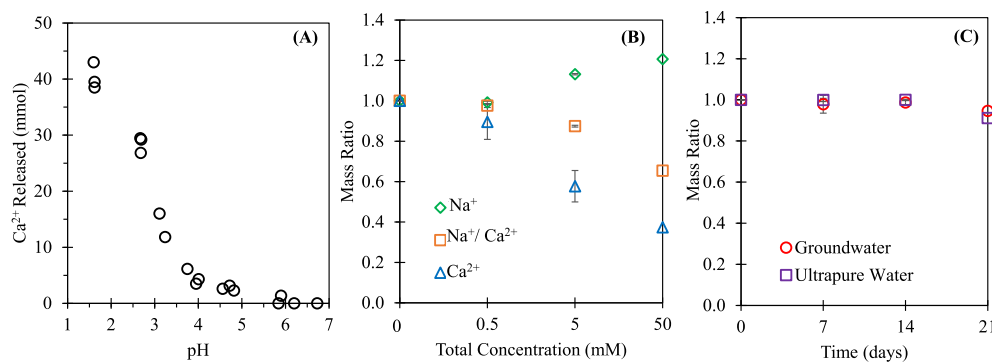
Fig. 7. Effects of aqueous phase conditions on the structural stability of the Ca-alginate hydrogel. (A) Quantity of Ca^{2+} released as a function of aqueous phase pH in Ca-alginate hydrogels with no Pd. (B) Mass ratio of Ca-alginate hydrogel after exposure to increasing total concentrations of monovalent, divalent, and mixed salt solutions. (C) Mass ratio of hydrogels over a 3-week period of exposure to ultrapure water and model groundwater. The error bars indicate the standard deviation of triplicate trials at the same condition.

and presumably small changes in the hydrogel mass ratio, either due to shrinking or swelling, will not significantly affect the reaction rate.

To investigate the changes in hydrogel swelling under relevant aqueous conditions, the mass-ratio of hydrogels was measured over 21 d in an ultrapure water or a groundwater (Fig. 7C). No significant hydrogel shrink/swell (<6% mass-ratio change) was observed over this period in either matrix, suggesting that hydrogel structural changes were minimal. The Na^+/Ca^{2+} molar ratio (10:6.1; 4.4 mM Na^+, 2.7 mM Ca^{2+}) and total [$Na^+ + Ca^{2+}$] concentration (7.1 mM) of the groundwater (Table S5) were similar to those for the model Na^+/Ca^{2+} mixture at 5 mM (4.4 mM Na^+, 0.61 mM Ca^{2+}). A comparable shrinking behavior between the two was observed with mass ratios of 0.94 and 0.87, respectively. The groundwater also contained 1.25 mM Mg^{2+}, which may have contributed to the crosslinking, although the affinity of alginate cross-link sites for Mg^{2+} is lower than Ca^{2+} (Idota et al., 2016).

The tendency of Pd-nanoparticles to leach from the catalytic hydrogel during the stability experiments was investigated by measuring Pd concentrations in the aqueous phase after the soaking period. Pd was only detected in the aqueous phase when concentrations of Na^+ greater than 50 mM were used. After exposure to a 50 mM Na^+ solution, only 2.5 μg (0.29%) of the total Pd present in the hydrogel was detected in the aqueous phase. Pd leaching is attributed to de-linking and swelling of hydrogel structure. When major hydrogel swelling was avoided, no detectable Pd leaching was observed. These results show that groundwaters are excellent candidates for the CHMR due to the presence of divalent cations that reduce hydrogel swelling. Source waters with high concentrations of monovalent cations and low concentrations of divalent cations (e.g., some surface waters) may need pretreatment (addition of Ca^{2+} salts) before the CHMR due to the expansion and degradation of the Ca-alginate hydrogel.

4. Conclusions

The CHMR is an effective system for immobilizing nano-sized catalysts to be used for the hydrogenation of oxidized contaminants. Pd and NO_2^- were used as models in this study because the synthesis of Pd and the hydrogenation pathway of NO_2^- are relatively straightforward. This simplicity allowed for key factors affecting the CHMR performance (e.g., influent reactant concentrations) to be evaluated without unnecessary complications (e.g., unknown intermediate reactions). The CHMR is adaptable to other catalysts and contaminants. For contaminants that are treatable using Pd [e.g., trichloroethylene (Lowry and Reinhard, 2000)], no changes to the catalytic hydrogel synthesis process would be

required. For contaminants that require alternative or more intricate catalysts, changes to the synthesis process could be easily implemented. For example, hydrogenation of nitrate (NO_3^-), an important drinking water contaminant, requires a more complex bimetallic catalyst such as Pd—In (Chaplin et al., 2012; Guo et al., 2018). The Pd catalyst used herein could be replaced with the Pd—In catalyst by adding a step in the catalytic hydrogel synthesis process to cover Pd with In, or the Pd—In catalysts could be synthesized ex-situ and then incorporated during the hydrogel crosslinking step. Similarly, an Re—Pd catalyst could be used to reduce perchlorate (ClO_4^-) (Liu et al., 2013). For all hydrogenation catalyst and contaminant scenarios, the reactivity will be affected similarly by the diffusion-reaction processes observed in this study. While the optimal operating conditions will change for each scenario, the important parameters controlling the overall rate that were explored herein (e.g., influent contaminant concentration, H_2 supply pressure, catalyst density) will be universal.

Due to diffusion, the steady-state concentrations of H_2 and NO_2^- will decrease with increasing distance from the bulk source, and thus the reaction rate at catalyst sites varies within the hydrogel. This affects the width of the reaction zone and highlights the need to optimize the catalytic hydrogel thickness. The 1-D model usedd herein for the CHMR is useful for predicting reaction profiles in the catalytic hydrogel and tuning its parameters. The needs to be calibrated using experimental data and expanded to evaluate important operating parameters such as flux. While the hydrogel afforded some protection from the catalyst deactivating species tested — especially larger molecules like DOM — smaller species remain a problem. Future studies are needed to better understand the molecular-scale interactions between Pd and naturally occurring deactivating species. These results could be used to engineer Pd catalysts more resistant to deactivation. Operationally, the H_2 usage efficiency can be optimized using a venting strategy, and the number of fibers can be increased to treat a wide range of flows and concentrations. Furthermore, the CHMR can use existing infrastructure designed for HFM membrane biofilm reactors. The use of H_2 as a reductant may contribute to biofilm grown on the catalytic hydrogel, but this can be mitigated by controlling the H_2 concentration so that it is zero at the bulk water interface. No biofilm growth was observed in this or previous studies (Marks et al., 2019), but this result should be confirmed under more conditions and for longer time periods.

Declaration of competing interest

The authors declare that they have no known competing financial interests or personal relationships that could have

appeared to influence the work reported in this paper.

Acknowledgements

Appendix A. Supplementary data

Supplementary data to this article can be found online at https://doi.org/10.1016/j.watres.2020.115593.

References

Ahmed, T., Semmens, M.J., Voss, M.A., 2004. Oxygen transfer characteristics of hollow-fiber, composite membranes. Adv. Environ. Res. 8 (3–4), 637–646.

Ai, L.H., Jiang, J., 2013. Catalytic reduction of 4-nitrophenol by silver nanoparticles stabilized on environmentally benign macroscopic biopolymer hydrogel. Bioresour. Technol. 132, 374–377.

Ai, L.H., Yue, H.T., Jiang, J., 2012. Environmentally friendly light-driven synthesis of Ag nanoparticles in situ grown on magnetically separable biohydrogels as highly active and recyclable catalysts for 4-nitrophenol reduction. J. Mater. Chem. 22 (44), 23447–23453.

Bajpai, S.K., Sharma, S., 2004. Investigation of swelling/degradation behaviour of alginate beads crosslinked with Ca2+ and Ba2+ ions. React. Funct. Polym. 59 (2), 129–140.

Bergquist, A.M., Choe, J.K., Strathmann, T.J., Werth, C.J., 2016. Evaluation of a hybrid ion exchange-catalyst treatment technology for nitrate removal from drinking water. Water Res. 96, 177–187.

Bertoch, M., Bergquist, A.M., Gildert, G., Strathmann, T.J., Werth, C.J., 2017. Catalytic nitrate removal in a trickle bed reactor: direct drinking water treatment. J. AWWA (Am. Water Works Assoc.) 109 (5), E144–E157.

Centi, G., Dittmeyer, R., Perathoner, S., Reif, M., 2003. Tubular inorganic catalytic membrane reactors: advantages and performance in multiphase hydrogenation reactions. Catal. Today 79 (1–4), 139–149.

Chaplin, B.P., Reinhard, M., Schneider, W.F., Schuth, C., Shapley, J.R., Strathmann, T.J., Werth, C.J., 2012. Critical review of Pd-based catalytic treatment of priority contaminants in water. Environ. Sci. Technol. 46 (7), 3655–3670.

Chaplin, B.P., Roundy, E., Guy, K.A., Shapley, J.R., Werth, C.J., 2006. Effects of natural water ions and humic acid on catalytic nitrate reduction kinetics using an alumina supported Pd-Cu catalyst. Environ. Sci. Technol. 40 (9), 3075–3081.

Chaplin, B.P., Shapley, J.R., Werth, C.J., 2009. Oxidative regeneration of sulfide-fouled catalysts for water treatment. Catal. Lett. 132 (1–2), 174–181.

Chen, H.Y., Lo, S.L., Ou, H.H., 2013. Catalytic hydrogenation of nitrate on Cu-Pd supported on titanate nanotube and the experiment after aging, sulfide fouling and regeneration procedures. Appl. Catal. B Environ. 142, 65–71.

Chen, P., Zhang, X.G., Mia, Z.J., Han, B.X., An, G.M., Liu, Z.M., 2009. In-situ synthesis of noble metal nanoparticles in alginate solution and their application in catalysis. J. Nanosci. Nanotechnol. 9 (4), 2628–2633.

Chinthaginjala, J.K., Bitter, J.H., Lefferts, L., 2010. Thin layer of carbon-nano-fibers (CNFs) as catalyst support for fast mass transfer in hydrogenation of nitrite. Appl. Catal. Gen. 383 (1–2), 24–32.

Choe, J.K., Bergquist, A.M., Jeong, S., Guest, J.S., Werth, C.J., Strathmann, T.J., 2015. Performance and life cycle environmental benefits of recycling spent ion exchange brines by catalytic treatment of nitrate. Water Res. 80, 267–280.

Chtchigrovsky, M., Lin, Y., Ouchaou, K., Chaumontet, M., Robitzer, M., Quignard, F., Taran, F., 2012. Dramatic effect of the gelling cation on the catalytic performances of alginate-supported palladium nanoparticles for the suzuki-miyaura reaction. Chem. Mater. 24 (8), 1505–1510.

Chuang, J.J., Huang, Y.Y., Lo, S.H., Hsu, T.F., Huang, W.Y., Huang, S.L., Lin, Y.S., 2017. Effects of pH on the shape of alginate particles and its release behavior. Int. J. Polymer Sci.

Daub, K., Emig, G., Chollier, M.J., Callant, M., Dittmeyer, R., 1999. Studies on the use of catalytic membranes for reduction of nitrate in drinking water. Chem. Eng. Sci. 54 (10), 1577–1582.

Davie, M.G., Cheng, H.F., Hopkins, G.D., Lebron, C.A., Reinhard, M., 2008. Implementing heterogeneous catalytic dechlorination technology for remediating TCE-contaminated groundwater. Environ. Sci. Technol. 42 (23), 8908–8915.

Dittmeyer, R., Hollein, V., Daub, K., 2001. Membrane reactors for hydrogenation and dehydrogenation processes based on supported palladium. J. Mol. Catal. Chem. 173 (1–2), 135–184.

Dittmeyer, R., Svajda, K., Reif, M., 2004. A review of catalytic membrane layers for gas/liquid reactions. Top. Catal. 29 (1–2), 3–27.

Draget, K.I., Skjak-Braek, G., Stokke, B.T., 2006. Similarities and differences between alginic acid gels and ionically crosslinked alginate gels. Food Hydrocolloids 20 (2–3), 170–175.

Espinosa, R.B., Lefferts, L., 2016. Ni in CNFs: highly active for nitrite hydrogenation. ACS Catal. 6 (8), 5432–5440.

Espinosa, R.B., Rafieian, D., Lammertink, R.G.H., Lefferts, L., 2016. Carbon nano-fiber based membrane reactor for selective nitrite hydrogenation. Catal. Today 273, 50–61.

Espinosa, R.B., Rafieian, D., Postma, R.S., Lammertink, R.G.H., Lefferts, L., 2018. Eggshell membrane reactors for nitrite hydrogenation: manipulating kinetics and selectivity. Appl. Catal. B Environ. 224, 276–282.

Fang, Y.L., Heck, K.N., Alvarez, P.J.J., Wong, M.S., 2011. Kinetics analysis of palladium/gold nanoparticles as colloidal hydrodechlorination catalysts. ACS Catal. 1 (2), 128–138.

Favre, E., Leonard, M., Laurent, A., Dellacherie, E., 2001. Diffusion of polyethyleneglycols in calcium alginate hydrogels. Colloid. Surface. Physicochem. Eng. Aspect. 194 (1–3), 197–206.

Francis, N.L., Hunger, P.M., Donius, A.E., Riblett, B.W., Zavaliangos, A., Wegst, U.G.K., Wheatley, M.A., 2013. An ice-templated, linearly aligned chitosan-alginate scaffold for neural tissue engineering. J. Biomed. Mater. Res. 101 (12), 3493–3503.

Garbayo, I., Leon, R., Vigara, J., Vilchez, C., 2002. Diffusion characteristics of nitrate and glycerol in alginate. Colloids Surf. B Biointerfaces 25 (1), 1–9.

Guo, S.J., Heck, K., Kasiraju, S., Qian, H.F., Zhao, Z., Grabow, L.C., Miller, J.T., Wong, M.S., 2018. Insights into nitrate reduction over indium-decorated palladium nanoparticle catalysts. ACS Catal. 8 (1), 503–515.

Heck, K.N., Garcia-Segura, S., Westerhoff, P., Wong, M.S., 2019. Catalytic converters for water treatment. Acc. Chem. Res. 52 (4), 906–915.

Heck, K.N., Nutt, M.O., Alvarez, P., Wong, M.S., 2009. Deactivation resistance of Pd/Au nanoparticle catalysts for water-phase hydrodechlorination. J. Catal. 267 (2), 97–104.

Hinshelwood, C.N.S., 1940. The Kinetics of Chemical Change. The Clarendon press, Oxford.

Holler, V., Radevik, K., Yuranov, I., Kiwi-Minsker, L., Renken, A., 2001. Reduction of nitrite-ions in water over Pd-supported on structured fibrous materials. Appl. Catal. B Environ. 32 (3), 143–150.

Horold, S., Tacke, T., Vorlop, K.D., 1993a. Catalytical removal of nitrate and nitrite from drinking-water 1. Screening for hydrogenation catalysts and influence OF reaction conditions on activity and selectivity. Environ. Technol. 14 (10), 931–939.

Horold, S., Vorlop, K.D., Tacke, T., Sell, M., 1993b. Development OF catalysts for a selective nitrate and nitrite removal from drinking-water. Catal. Today 17 (1–2), 21–30.

Hu, M.C., Liu, Y., Yao, Z.H., Ma, L.P., Wang, X.Q., 2018. Catalytic reduction for water treatment. Front. Environ. Sci. Eng. 12 (1).

Huai, L.Y., He, C.Z., Wang, H., Wen, H., Yi, W.C., Liu, J.Y., 2015. NO dissociation and reduction by H-2 on Pd(111): a first-principles study. J. Catal. 322, 73–83.

Huang, J.F., Li, Y.T., Wu, J.H., Dong, X.M., Cao, P.Y., Liu, Y.L., Lin, Z.T., Jiang, G.B., 2016. Facile preparation of amorphous iron nanoparticles filled alginate matrix composites with high stability. Compos. Sci. Technol. 134, 168–174.

Idota, Y., Kogure, Y., Kato, T., Yano, K., Arakawa, H., Miyajima, K., Kasahara, F., Ogihara, T., 2016. Relationship between physical parameters of various metal ions and binding affinity for alginate. Biol. Pharmaceut. Bull. 39 (11), 1893–1896.

Jani, J.M., Aran, H.C., Wessling, M., Lammertink, R.G.H., 2012. Modeling of gas-liquid reactions in porous membrane microreactors. J. Membr. Sci. 419, 57–64.

Jarrah, N., 2018. Nitrite hydrogenation over palladium-carbon nanofiber foam: a parametric study using factorial design of experiments. React. Kinet. Mech. Catal. 125 (1), 287–301.

Lee, K.Y., Mooney, D.J., 2012. Alginate: properties and biomedical applications. Prog. Polym. Sci. 37 (1), 106–126.

Li, H., Guo, S.J., Shin, K., Wong, M.S., Henkelman, G., 2019. Design of a Pd-Au nitrite reduction catalyst by identifying and optimizing active ensembles. ACS Catal. 9 (9), 7957–7966.

Li, S.J., Fang, Y.L., Romanczuk, C.D., Jin, Z.H., Li, T.L., Wong, M.S., 2012. Establishing the trichloroethene dechlorination rates of palladium-based catalysts and iron-based reductants. Appl. Catal. B Environ. 125, 95–102.

Li, Y., Li, G., Li, W., Yang, F., Liu, H.H., 2015. Greenly synthesized gold-alginate nanocomposites catalyst for reducing decoloration of azo-dyes. Nano 10 (8).

Liu, J.Y., Choe, J.K., Sasnow, Z., Werth, C.J., Strathmann, T.J., 2013. Application of a Re-Pd bimetallic catalyst for treatment of perchlorate in waste ion-exchange regenerant brine. Water Res. 47 (1), 91–101.

Loureiro dos Santos, L.A., 2017. Natural Polymeric Biomaterials: Processing and Properties. Elsevier.

Lowry, G.V., Reinhard, M., 2000. Pd-catalyzed TCE dechlorination in groundwater: solute effects, biological control, and oxidative catalyst regeneration. Environ. Sci. Technol. 34 (15), 3217–3223.

Mahmudov, R., Shu, Y., Rykov, S., Chen, J., Huang, C.P., 2008. The reduction of perchlorate by hydrogenation catalysts. Appl. Catal. B Environ. 81 (1–2), 78–87.

Marks, R., Seaman, J., Perez-Calleja, P., Kim, J., Nerenberg, R., Doudrick, K., 2019. Catalytic hydrogel membrane reactor for treatment of aqueous contaminants. Environ. Sci. Technol. 53 (11), 6492–6500.

Martin, K.J., Nerenberg, R., 2012. The membrane biofilm reactor (MBfR) for water

and wastewater treatment: principles, applications, and recent developments. Bioresour. Technol. 122, 83—94.

Martin, K.J., Picioreanu, C., Nerenberg, R., 2013. Multidimensional modeling of biofilm development and fluid dynamics in a hydrogen-based, membrane biofilm reactor (MBfR). Water Res. 47 (13), 4739—4751.

Martin, K.J., Picioreanu, C., Nerenberg, R., 2015. Assessing microbial competition in a hydrogen-based membrane biofilm reactor (MBfR) using multidimensional modeling. Biotechnol. Bioeng. 112 (9), 1843—1853.

Martinez, J., Ortiz, A., Ortiz, I., 2017. State-of-the-art and perspectives of the catalytic and electrocatalytic reduction of aqueous nitrates. Appl. Catal. B Environ. 207, 42—59.

Matatov-Meytal, U., Sheintuch, M., 2005. Activated carbon cloth-supported Pd-Cu catalyst: application for continuous water denitrification. Catal. Today 102, 121—127.

Matatov-Meytal, U., Sheintuch, M., 2009. The relation between surface composition of Pd-Cu/ACC catalysts prepared by selective deposition and their denitrification behavior. Catal. Commun. 10 (8), 1137—1141.

Matatov-Meytal, Y., Barelko, V., Yuranov, I., Kiwi-Minsker, L., Renken, A., Sheintuch, M., 2001. Cloth catalysts for water denitrification II. Removal of nitrates using Pd-Cu supported on glass fibers. Appl. Catal. B Environ. 31 (4), 233—240.

Matatov-Meytal, Y., Barelko, V., Yuranov, I., Sheintuch, M., 2000. Cloth catalysts in water denitrification - I. Pd on glass fibers. Appl. Catal. B Environ. 27 (2), 127—135.

Matatov-Meytal, Y., Shindler, Y., Sheintuch, M., 2003. Cloth catalysts in water denitrification - III. pH inhibition of nitrite hydrogenation over Pd/ACC. Appl. Catal. B Environ. 45 (2), 127—134.

Matyash, M., Despang, F., Ikonomidou, C., Gelinsky, M., 2014. Swelling and mechanical properties of alginate hydrogels with respect to promotion of neural growth. Tissue Eng. C Methods 20 (5), 401—411.

Nakayama, N., Takahashi, M., 2015. Catalytic hydrogenation of nitrate in water using a Pd-Cu/Al2O3 catalyst and dilute H-2 microbubbles. Catal. Lett. 145 (9), 1756—1763.

Nerenberg, R., 2016. The membrane-biofilm reactor (MBfR) as a counter-diffusional biofilm process. Curr. Opin. Biotechnol. 38, 131—136.

Nutt, M.O., Hughes, J.B., Wong, M.S., 2005. Designing Pd-on-Au bimetallic nanoparticle catalysts for trichloroethene hydrodechlorination. Environ. Sci. Technol. 39 (5), 1346—1353.

Pankhania, M., Stephenson, T., Semmens, M.J., Inst Chem, E., 1994. Hollow fibre bioreactor for wastewater treatment using BUBBLELESS membrane aeration. In: 1994 Icheme Research Event, vols. 1 and 2, pp. 356—358.

Pasut, E., Toffanin, R., Voinovich, D., Pedersini, C., Murano, E., Grassi, M., 2008. Mechanical and diffusive properties of homogeneous alginate gels in form of particles and cylinders. J. Biomed. Mater. Res. 87A (3), 808—818.

Perez-Calleja, P., Aybar, M., Picioreanu, C., Esteban-Garcia, A.L., Martin, K.J., Nerenberg, R., 2017. Periodic venting of MABR lumen allows high removal rates and high gas-transfer efficiencies. Water Res. 121, 349—360.

Pintar, A., Batista, J., 2007. Catalytic stepwise nitrate hydrogenation in batch-recycle fixed-bed reactors. J. Hazard Mater. 149 (2), 387—398.

Pintar, A., Batista, J., Levec, J., Kajiuchi, T., 1996. Kinetics of the catalytic liquid-phase hydrogenation of aqueous nitrate solutions. Appl. Catal. B Environ. 11 (1), 81—98.

Pintar, A., Bercic, G., Levec, J., 1998. Catalytic liquid-phase nitrite reduction: kinetics and catalyst deactivation. AIChE J. 44 (10), 2280—2292.

Postma, R.S., Espinosa, R.B., Lefferts, L., 2018. Competitive adsorption of nitrite and

hydrogen on palladium during nitrite hydrogenation. ChemCatChem 10 (17), 3770—3776.

Prusse, U., Vorlop, K.D., 2001. Supported bimetallic palladium catalysts for water-phase nitrate reduction. J. Mol. Catal. Chem. 173 (1—2), 313—328.

Puguan, J.M.C., Yu, X.H., Kim, H., 2015. Diffusion characteristics of different molecular weight solutes in Ca-alginate gel beads. Colloid. Surface. Physicochem. Eng. Aspect. 469, 158—165.

Qian, H.F., Zhao, Z., Velazquez, J.C., Pretzer, L.A., Heck, K.N., Wong, M.S., 2014. Supporting palladium metal on gold nanoparticles improves its catalysis for nitrite reduction. Nanoscale 6 (1), 358—364.

Qiao, X.L., Niu, L.B., Zhang, H.L., Wen, X., Cao, Y.Y., Bai, G.Y., 2017. Controllable fabrication of a novel porous Ni-alginate hybrid material for hydrogenation. Appl. Catal. B Environ. 218, 721—730.

Saha, S., Pal, A., Kundu, S., Basu, S., Pal, T., 2010. Photochemical green synthesis of calcium-alginate-stabilized Ag and Au nanoparticles and their catalytic application to 4-nitrophenol reduction. Langmuir 26 (4), 2885—2893.

Seraj, S., Kunal, P., Li, H., Henkelman, G., Humphrey, S.M., Werth, C.J., 2017. PdAu alloy nanoparticle catalysts: effective candidates for nitrite reduction in water. ACS Catal. 7 (5), 3268—3276.

Shelstad, K.A., Downie, J., Graydon, W.F., 1960. Kinetics of the vapor-phase oxidation of napthalene over a vanadium catalyst. Can. J. Chem. Eng. (August), 102—107.

Shuai, D.M., McCalman, D.C., Choe, J.K., Shapley, J.R., Schneider, W.F., Werth, C.J., 2013. Structure sensitivity study of waterborne contaminant hydrogenation using shape- and size-controlled Pd nanoparticles. ACS Catal. 3 (3), 453—463.

Soares, O.S.G.P., Orfao, J.J.M., Pereira, M.F.R., 2008. Activated carbon supported metal catalysts for nitrate and nitrite reduction in water. Catal. Lett. 126 (3—4), 253—260.

Strukul, G., Gavagnin, R., Pinna, F., Modaferri, E., Perathoner, S., Centi, G., Marella, M., Tomaselli, M., 2000. Use of palladium based catalysts in the hydrogenation of nitrates in drinking water: from powders to membranes. Catal. Today 55 (1—2), 139—149.

Thangaraj, V., Mahmud, S., Li, W., Yang, F., Liu, H.H., 2018. Greenly synthesised silver-alginate nanocomposites for degrading dyes and bacteria. IET Nanobiotechnol. 12 (1), 47—51.

Vorlop, K.D., Tacke, T., 1989. 1ST steps towards noble-metal catalyzed removal OF nitrate and nitrite from drinking-water. Chem. Ing. Tech. 61 (10), 836—837.

Wong, M.S., Alvarez, P.J.J., Fang, Y.L., Akcin, N., Nutt, M.O., Miller, J.T., Heck, K.N., 2009. Cleaner water using bimetallic nanoparticle catalysts. J. Chem. Technol. Biotechnol. 84 (2), 158—166.

Xiao, T.C., An, L.D., Zhang, W.M., Sheng, S.S., Xiong, G.X., 1992. Mechanism of sulfur poisoning on supported noble-metal catalyst - the adsorption and transformation of sulfur on palladium catalysts with different supports. Catal. Lett. 12 (1—3), 287—296.

Xuan, C., Wu, Z., Lei, W., Wang, J., Guo, J., Wang, D., 2017. Nitrogen-doped hierarchical porous carbons derived from sodium alginate as efficient oxygen reduction reaction electrocatalysts. ChemCatChem 9 (5), 809—815.

Yoshinaga, Y., Akita, T., Mikami, I., Okuhara, T., 2002. Hydrogenation of nitrate in water to nitrogen over Pd-Cu supported on active carbon. J. Catal. 207 (1), 37—45.

Zhao, Y.N., Rao, N.K., Lefferts, L., 2016. Adsorbed species on Pd catalyst during nitrite hydrogenation approaching complete conversion. J. Catal. 337, 102—110.

Zhao, Z., Fang, Y.L., Alvarez, P.J.J., Wong, M.S., 2013. Degrading perchloroethene at ambient conditions using Pd and Pd-on-Au reduction catalysts. Appl. Catal. B Environ. 140, 468—477.